

# Length Estimation in 3-D Using Cube Quantization

Amnon Jonas\* and Nahum Kiryati†

Department of Electrical Engineering  
Technion - Israel Institute of Technology  
Haifa 32000, Israel

## Abstract

Estimators for the original length of a continuous 3-D curve given its digital representation are developed. The 2-D case has been extensively studied. The few estimators that have been suggested for 3-D curves suffer from serious drawbacks, partly due to incomplete understanding of the characteristics of digital representation schemes for 3-D curves.

The selection and thorough understanding of the digital curve representation scheme is crucial to the design of 3-D length estimators. A comprehensive study on the digitization of 3-D curves was recently carried out. It was shown that grid intersect quantization and other 3-D curve discretization schemes that lead to 26-directional chain codes do not satisfy several fundamental requirements, and that cube quantization, that leads to 6-directional chain codes, should be preferred.

The few 3-D length estimators that have been suggested are based on 26-directional chain coding that naturally provides a classification of the chain links which is necessary for accurate length estimation. Cube quantization is mathematically well-behaved but the symmetry and uniformity of the 6-directional digital chain elements create a challenge in their classification for length estimation.

In this paper length estimators for 3-D curves digitized using cube quantization are developed. Simple but powerful link classification criteria for 6-directional digital curves are presented. They are used to obtain unbiased length estimators, with RMS errors as low as 0.57% for randomly oriented straight lines, about five times better than in the best estimators that have been so far available.

---

\*Currently with RDC Communications Ltd., P.O.Box 34233, Jerusalem 91341, Israel

†To whom correspondence should be addressed

# 1 Introduction

Suppose that a continuous curve in three dimensional space has been quantized and is given in digital form, e.g. as a 3-D chain code. Can the length of the original continuous curve be recovered? Since information is lost in the digitization process, the answer is no. Each digital curve could have been obtained from an infinite number of continuous curves. Unique reconstruction, and length recovery, are thus impossible.

Had the set of continuous curves that have the same digital representation been roughly similar in shape and length, the original length could have been estimated to be some average of the lengths of continuous curves in that set. However, in such a set there are continuous curves that exhibit sub-voxel fractal behavior that is not captured by the digitization process. The existence of such curves, including curves of infinite length, precludes meaningful length estimation by set averaging.

In any practical image analysis system quantization must be sufficiently fine to capture the essential shapes of objects to be analyzed (at the relevant scale). Then, for practical purposes, curves can be considered smooth except at a small number of corners. If the curves can be assumed to be nearly straight in small neighborhoods around most of the digital curve points, meaningful length estimation becomes possible.

The 2-D length estimation problem has received considerable attention. Relatively recent references are [4, 14]. The standard approach to length estimation is to classify the chain code elements according to certain criteria, and estimate the length as a weighted sum of the number of chain elements in each class. Once the classification criteria are selected, the corresponding weights are designed to yield unbiased and in some sense optimal estimates of the length of straight lines. Unbiasedness for straight lines implies that when applied to general curves with varying tangent orientations, local length estimation errors are likely to cancel out, and excellent total length estimation can be expected.

The increasing importance of three dimensional shape analysis in medical imaging, range image processing, navigation and other domains has recently led to interest in the development of length estimators for digitized 3-D curves. The few estimators that have been suggested are based on 26-directional chain code representation of the digital curve. That representation provides natural classification of the chain code links to three classes, which is very convenient for length estimation. Certain methods [1, 3] rely on global properties of digital straight lines and are thus applicable only to straight lines and cannot be extended to estimating the length of general curves. The work of Verwer [18] deals with the design of local weights for distance transformations. Kiryati and Székely [15] have however observed that in 3-D, the shortest digital path between two voxels obtained by a search algorithm in a chamfer distance transformation is not necessarily a digital straight line (i.e., the digitization of a continuous straight line) that passes through two voxels. This leads to a fundamental difference between the design of length estimators and of local weights for Euclidean distance transformations

in 3-D. That distinction is missing in reference [2]. That paper too should be regarded as dealing with distance transformations rather than length estimation. An estimator of the length of a continuous 3-D curve given its thinned cube quantization (TCQ) representation (see section 3) has been presented by Kiryati and Kübler [11].

The cumulative experience in 3-D length estimation thus indicates that thorough understanding of 3-D digital curve representation is crucial for the development of valid and accurate 3-D length estimators. The extension of 2-D curve digitization schemes to 3-D is surprisingly nontrivial and important properties of 3-D schemes are unobvious and somewhat counterintuitive.

Reference [9] is a comprehensive study of digital representation schemes for 3-D curves. In that paper the concept of a mathematically “well-behaved” 3-D curve representation scheme is formalized and summarized as a list of requirements. Those are used as a basis for qualitative and quantitative comparison of various methods. It is shown that 3-D grid intersect quantization and other 3-D schemes that lead to 26-connected chain codes have serious drawbacks and that cube quantization, an extension of 2-D square quantization to 3-D, that leads to 6-connected chain codes, meets all the identified requirements and should be preferred.

In this paper we develop length estimators that are based on cube quantization. Unlike 26-directional chain elements that are of three types, 6-directional chain elements are symmetric, and uniform. The first challenge is therefore to obtain link classification criteria for 6-directional digital curves that are simple, local but sufficiently powerful to allow accurate length estimation. Three unbiased length estimators are then developed. First a so-called one sided estimator that is the basis for a greatly superior two sided estimator, with RMS error of 0.57% for equally distributed straight lines. This is about five times better than in previous estimators. The above two estimators rely on the availability of the chain code representation of the curve, i.e., on knowing the order of the digital points along the curve. We also present a high performance estimator that does not require ordered chain code input and can operate directly on the digital image of the curve.

The organization of the paper is as follows. A generic mathematical framework for the development of length estimators is described in section 2. The properties and advantages of cube quantization are summarized in section 3. The derivation of the three suggested estimators is straight-forward, but cumbersome. Therefore the main results are summarized in a self-contained form in section 4. The detailed analysis is presented in sections 5, 6 and 7. Experimental results that corroborate and complement the analysis are provided in section 8, followed by a discussion (section 9). Reference [8] is a preliminary version of this paper.

## 2 Mathematical Framework for 3-D Length Estimation

This section describes a general mathematical framework for estimating the length of a continuous 3-D curve given its digital representation. The description is general in the sense that the criteria for classifying the chain elements are not specified: different criteria lead to different estimators. A similar approach was used by Kiryati and Kübler [11]. It is an extension to 3-D of 2-D perimeter estimation techniques, see e.g. [14].

Let  $l(t)$  be a three dimensional straight line:

$$l(t) = [x(t), y(t), z(t)] \quad (1)$$

and assume that its digital representation scheme is symmetric with respect to the axes. Then, without loss of generality, the discussion can be focused on lines that satisfy

$$\frac{dx}{dt} \geq \frac{dy}{dt} \geq \frac{dz}{dt} \geq 0. \quad (2)$$

For a line in general position, the probability for an equality in Eq. (2) is zero, hence this case is not further discussed and it is assumed that

$$\frac{dx}{dt} > \frac{dy}{dt} > \frac{dz}{dt} > 0. \quad (3)$$

This consideration is also applied in the sequel.

Define

$$a = \frac{dy}{dx} \quad b = \frac{dz}{dx} \quad (4)$$

$$y_0 = y(t)|_{x(t)=0} \quad z_0 = z(t)|_{x(t)=0} \quad (5)$$

Then

$$y = ax + y_0 \quad z = bx + z_0 \quad (6)$$

Assume that the digital curve representation scheme is invariant to integer translations. Then without loss of generality the origin can be placed such that

$$1 > a > b > 0 \quad 0 < y_0 < 1 \quad 0 < z_0 < 1 \quad (7)$$

The length estimation problem is to estimate the original length of a curve in the preimage given its digital representation. Suppose that one classifies the chain elements (digital curve points or chain links) to  $k$  mutually exclusive groups  $\Omega_1, \Omega_2, \dots, \Omega_k$ . Let  $N_i$  denote the number of elements in  $\Omega_i$ . The general form of a linear length estimator that is based on this classification is

$$\hat{L} = \sum_{i=1}^k \Psi_i N_i, \quad (8)$$

where the weight  $\Psi_i$  is the contribution of an element in  $\Omega_i$  to the estimated curve length.

Applying this estimator to the straight line  $l$  and assuming that its actual length  $L$  is large, the estimation error is

$$\epsilon(l) = \lim_{L \rightarrow \infty} \frac{\hat{L} - L}{L} = \lim_{L \rightarrow \infty} \frac{1}{L} \sum_{i=1}^k \Psi_i N_i - 1. \quad (9)$$

Define

$$P_i(l) = \lim_{L \rightarrow \infty} \frac{N_i}{L}, \quad (10)$$

then

$$\epsilon(l) = \sum_{i=1}^k P_i(l) \Psi_i - 1. \quad (11)$$

For almost all lines (except a zero measure set) the numbers  $1, a, b$  are independent above the integers. Then the length estimation error depends on the orientation of the line, i.e., on the slopes  $a, b$  but not on the intercepts  $y_0, z_0$ . Hence  $\epsilon(l)$  can be expressed as  $\epsilon(a, b)$ .

To obtain an unbiased estimator, it is required that the average error for a uniform distribution of line orientations will be zero:

$$\bar{\epsilon} = \frac{1}{c} \int_{a=0}^1 \int_{b=0}^a \epsilon(l) d\Omega = 0, \quad (12)$$

where  $d\Omega$  is the differential solid angle element and  $c$  is a normalization constant:

$$c = \int_{a=0}^1 \int_{b=0}^a d\Omega. \quad (13)$$

Substituting (11) in (12) gives

$$\bar{\epsilon} = \frac{1}{c} \left( \sum_{i=1}^k \Psi_i \int_{a=0}^1 \int_{b=0}^a P_i d\Omega \right) - 1 = 0. \quad (14)$$

Defining

$$c_i = \frac{1}{c} \int_{a=0}^1 \int_{b=0}^a P_i d\Omega \quad (15)$$

we obtain the unbiasedness requirement

$$\bar{\epsilon} = \sum_{i=1}^k \Psi_i c_i - 1 = 0. \quad (16)$$

The mean square length estimation error is

$$\epsilon_{MSE} = \frac{1}{c} \int_{a=0}^1 \int_{b=0}^a \epsilon^2(l) d\Omega. \quad (17)$$

The optimal (in the MSE sense) unbiased estimator can be obtained by using Lagrange multipliers for the minimization of  $\epsilon_{MSE}$  subject to the unbiasedness constraint Eq. (16). We define the Lagrangian

$$T = \epsilon_{MSE} + \lambda \bar{\epsilon} \quad (18)$$

and obtain the following system of equations:

$$\begin{cases} \frac{\partial T}{\partial \Psi_i} = 0 & i = 1, 2, \dots, k \\ \frac{\partial T}{\partial \lambda} = 0 \end{cases} \quad (19)$$

Differentiation gives

$$\frac{\partial T}{\partial \Psi_i} = \frac{\partial \epsilon_{MSE}}{\partial \Psi_i} + \lambda \frac{\partial \bar{\epsilon}}{\partial \Psi_i} \quad (20)$$

$$= \frac{1}{c} \int_{a=0}^1 \int_{b=0}^a 2\epsilon \frac{\partial \epsilon}{\partial \Psi_i} d\Omega + \lambda c_i \quad (21)$$

$$= \frac{2}{c} \sum_{j=1}^k \Psi_j \int_{a=0}^1 \int_{b=0}^a P_i P_j d\Omega - \frac{2}{c} \int_{a=0}^1 \int_{b=0}^a P_i d\Omega + \lambda c_i \quad (22)$$

and

$$\frac{\partial T}{\partial \lambda} = \bar{\epsilon} = \sum_{j=1}^k \Psi_j \frac{1}{c} \int_{a=0}^1 \int_{b=0}^a P_j d\Omega - 1. \quad (23)$$

Using Eq. (15) and the notation

$$\alpha_{ij} = \frac{2}{c} \int_{a=0}^1 \int_{b=0}^a P_i P_j d\Omega \quad (24)$$

we obtain a system of linear equations:

$$\begin{cases} \sum_{j=1}^k \alpha_{ij} \Psi_j + c_i \lambda = 2c_i, & i = 1, 2, \dots, k \\ \sum_{j=1}^k c_j \Psi_j = 1 \end{cases} \quad (25)$$

The solution of this system gives the weights that should be used in Eq. (8) to obtain the optimal (in the MSE sense) unbiased linear length estimator. This approach is used for the development of 3-D length estimators in the sequel.

### 3 Cube Quantization

The properties and advantages of cube quantization over other 3-D digital curve representation schemes have been studied in [9]. A brief summary is provided in this section.

Square Quantization [5, 6, 13] is a scheme for digital representation of 2-D curves. The image plane is divided to square pixels and the curve is implicitly segmented according to its intersections with the square pixels. The digital representation is the sequence of points at the centers of these pixels, following the order of the segments along the curve. For a curve in general position, the probability of corner crossing between pixels is zero and can be ignored, so diagonal links do not appear and a 4-chain is obtained. Other 2-D schemes can be used to get 8-chains. In Grid Intersection Quantization (GIQ) [5, 6] the curve is represented by selecting, at each intersection of the curve with a grid line, the closer grid point. The order of points follows the order of intersections along the curve.

Cube Quantization (CQ) is an extension of Square Quantization to 3-D in which cubic voxels replace square pixels and the digital curve representation is a 6-chain, see Fig. 1. Grid Intersect Quantization (GIQ) can also be extended to 3-D [10, 12] and leads to 26-chains. In 3-D GIQ, for each intersection of the curve with a grid *plane*, one selects the closest of the four grid points. Several properties of 3-D GIQ are presented in [10], extended to multi-dimensions in [12] (and used in [3]), but as shown by Stojmenović and Tošić[17], not all are correct. In particular, as stated in the sequel, 3-D GIQ does not satisfy the line-to-arc and projection properties.

A method used in [11] is referred to here as Thinned Cube Quantization (TCQ). The 26-chain obtained by that method is a subset of the 6-chain points obtained by Cube Quantization. The chain begins with the first Cube Quantization point and at each stage proceeds to the furthest possible point subject to maintaining 26 connectivity.

In an attempt to formalize and summarize the vague concept of a mathematically well-behaved 3-D curve representation scheme the following list of requirements has been suggested in [9].

- (a) Coordinate system axis symmetry - The quantization should be symmetric with respect to changes in the labels and directions of the axes.
- (b) Curve direction symmetry - Reversing the starting point and end point of the continuous curve should lead to the same chain in reversed order.
- (c) Invariance to integer translation - Integer translation of the continuous curve (or equivalently of the coordinate system origin) should lead to the same chain translated.
- (d) Finite memory - The representation of a curve segment should not depend on arbitrarily distant segments.

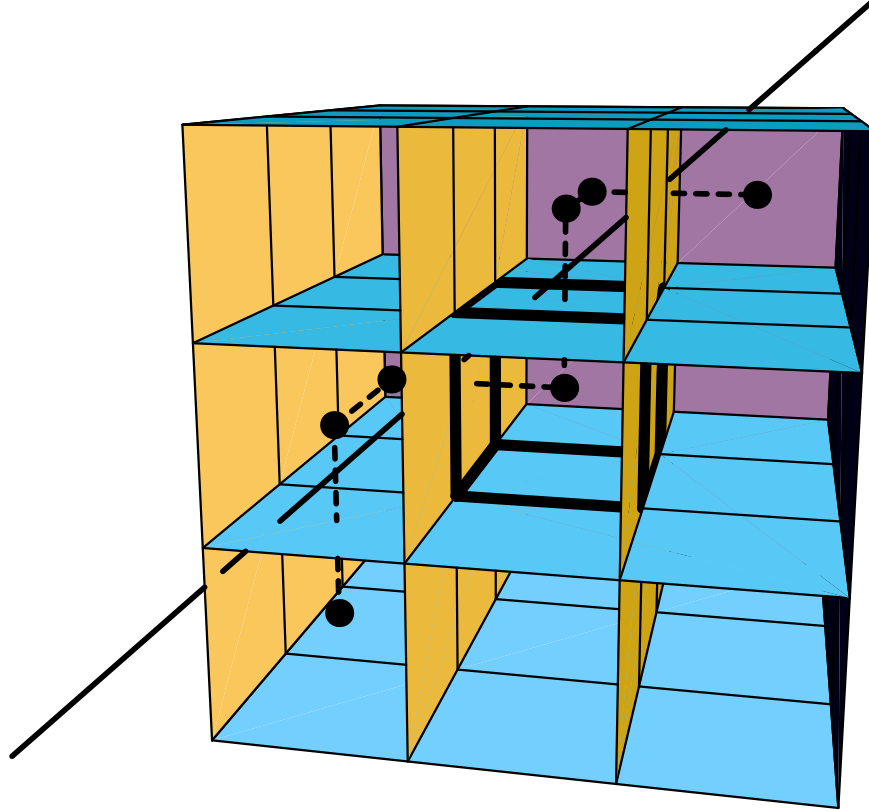


Figure 1: The Cube Quantization method for 3-D digital curve representation is a generalization of 2-D Square Quantization.

- (e) Line to arc - The discrete representation of a straight line should be a digital arc. This requirement is necessary for minimization of the number of elements (subject to maintaining connectivity) in the discrete chain. Since the shortest chain between two lattice points is necessarily a digital arc, it is reasonable to require that a digital straight line should be a digital arc.
- (f) The projection property - Let  $R_{ij}x$  be the projection of a 3-D curve or chain onto the  $ij$  plane, where  $i, j$  are any two coordinate axes. Let  $Q$  denote the quantization operator. The projection property is that  $QR_{ij}l = R_{ij}Ql$ , i.e., the projection of a 3-D chain onto a plane perpendicular to any one of the coordinate system axes should be identical to the 2-D digital representation of the projection of the continuous curve onto that plane.

Table 1 compares Grid Intersect Quantization (GIQ), Thinned Cube Quantization (TCQ)

and Cube Quantization (CQ) with respect to requirements (a) through (f). The qualitative superiority of cube quantization over GIQ and TCQ is apparent. In [9] it is also shown that cube quantization compares well with the other schemes with respect to the minimization of the distance between the discrete chain and the original continuous curve and with respect to the compactness of representation (in terms of bits).

<i>criterion</i>	CQ	GIQ	TCQ
a: coordinate system axes symmetry	+	+	+
b: curve direction symmetry	+	+	-
c: invariance to integer translation	+	+	+
d: finite memory	+	+	-
e: line to arc	+	-	+
f: the projection property	+	-	-

Table 1: Qualitative comparison of 3-D digital curve representation schemes.

## 4 Overview of the Main Results

The key to the design of linear length estimators is the ability to classify the digital curve points using simple criteria that reflect to local contribution to the length of the curve. 3-D digital curve representation schemes that lead to 26-directional chain codes are problematic in many respects, but allow very convenient link classification according to the three natural classes (direct, minor diagonal and major diagonal). Here length estimators that are based on Cube Quantization are developed. Cube quantization is mathematically well-behaved but the symmetry and uniformity of the 6-directional digital chain elements create a challenge in their classification for length estimation. The classification rules that are presented in the sequel are based on the number of digital curve points in the 26-neighborhood of a given digital curve point.

Consider a three dimensional curve and suppose that it is represented as a chain of voxels, using Cube Quantization. For classification, define the groups  $\Omega_1^{(1)}, \Omega_2^{(1)}, \Omega_3^{(1)}$  such that a voxel in the chain belongs to  $\Omega_m^{(1)}$  if exactly  $m$  immediately preceding voxels in the chain are in its 26-neighborhood (Fig. 2). A voxel in a digital straight line must belong to one of the three groups. A voxel in a general curve can have more than three immediately preceding voxels in its 26-neighborhood and in that case would not belong to any of these groups. In the development of the estimator it is assumed that the curve is usually smooth with respect to the quantization lattice, hence such voxels would be rare.

The optimal (in the MSE sense) unbiased linear estimator based on this classification

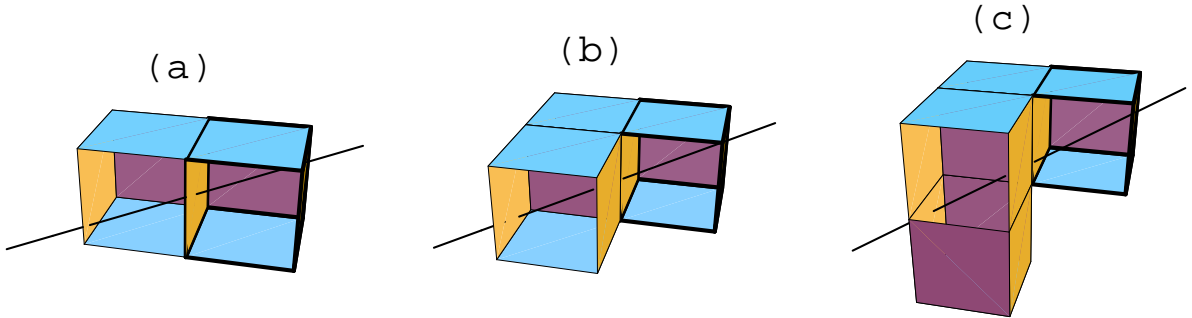


Figure 2: In the one-sided estimator the digital curve voxels are classified according to the number of preceding digital curve voxels in their 26-neighborhood. In (a), the highlighted voxel has a single preceding 26-neighbor, and belongs to  $\Omega_1$ . In (b), the highlighted voxel has two preceding 26-neighbors, and belongs to  $\Omega_2$ . In (c), the highlighted voxel has three preceding 26-neighbors, and belongs to  $\Omega_3$ . For the special case of straight lines, these are all the possible cases, and the links connecting the voxels within the 26-neighborhood include a single link at most in the direction of each coordinate axis.

is obtained in section 5 using the general approach outlined in the previous section. It is referred to as the *one-sided estimator*. The derivation is nontrivial and includes somewhat cumbersome geometric and algebraic steps. The optimal estimator is

$$\hat{L}_1 = 0.89710N_1^{(1)} + 0.65485N_2^{(1)} + 0.54218N_3^{(1)}. \quad (26)$$

The RMS error for straight lines is 2.49%. The importance of this estimator is not in the RMS error, which is comparable to the RMS errors attributed to previously suggested estimators, but in being based on Cube Quantization and in being the foundation for the highly accurate estimators presented in the sequel.

The one-sided estimator can be improved by separately counting the number of immediately preceding digital curve voxels and the number of immediately succeeding digital curve voxels in the 26-neighborhood of any digital curve voxel. These refined classification groups are denoted  $\Omega_{rs}^{(2)}$  ( $r \leq s$ ): a digital curve voxel belongs to  $\Omega_{rs}^{(2)}$  if exactly  $r$  immediately preceding voxels in the chain and  $s$  immediately succeeding voxels, or vice versa, are in its 26-neighborhood.

The optimal (in the MSE sense) unbiased linear estimator based on this refined classification is obtained in section 6. Again, the derivation turns out to be somewhat cumbersome. The result is

$$\hat{L}_2 = 0.98817N_{11}^{(2)} + 0.77296N_{12}^{(2)} + 0.62154N_{13}^{(2)} + 0.69037N_{22}^{(2)} + 0.60158N_{23}^{(2)} + 0.56782N_{33}^{(2)} \quad (27)$$

This is referred to as the *two-sided estimator*. Here the RMS error for straight lines is 0.57%, about five times better than in previously available estimators. The outstanding accuracy of this estimator is especially noteworthy since the classification is based just on the 26-neighborhood of the digital curve voxels.

Consider the classification groups  $\Omega_m^{(3)}$  defined such that a digital curve voxel is in  $\Omega_m^{(3)}$  if exactly  $m$  of the digital curve voxels are in its 26-neighborhood. For smooth original curves without digital self intersections, the following relations to the classification groups  $\Omega_{rs}^{(2)}$  that are used in the two-sided estimator hold:

$$\begin{aligned}\Omega_2^{(3)} &= \Omega_{11}^{(2)} \\ \Omega_3^{(3)} &= \Omega_{12}^{(2)} \\ \Omega_4^{(3)} &= \Omega_{13}^{(2)} \cup \Omega_{22}^{(2)} \\ \Omega_5^{(3)} &= \Omega_{23}^{(2)} \\ \Omega_6^{(3)} &= \Omega_{33}^{(2)}\end{aligned}\tag{28}$$

Using these classification groups for length estimation, the optimal estimator is:

$$\hat{L}_3 = 0.981111N_2^{(3)} + 0.77539N_3^{(3)} + 0.66483N_4^{(3)} + 0.60050N_5^{(3)} + 0.56479N_6^{(3)}\tag{29}$$

The RMS error for uniformly distributed straight lines is 1.13%. This estimator is unique in the sense that it does not need the digital curve voxels to be ordered in a chain, and can operate directly on the 3-D digital image. Its RMS error is twice as that of the two-sided estimator, but still significantly superior than that of any other previously available estimator. In applying this estimator one should be aware that since it is assumed that the ordering of the digital curve voxels is unknown, then if the curve intersects itself (or is close to that), the contribution of voxels near the intersection to the length estimate will be biased.

## 5 One Sided Length Estimator

Let  $l(t)$  be a three dimensional straight line and let  $V$  be a voxel through which the line passes. Without loss of generality set a coordinate system  $X, Y, Z$  such that the voxel  $V$  is at  $[0, 1]^3$ , the line enters the voxel at the face that coincides with the  $X = 0$  plane, and the following inequalities hold:

$$\frac{dX}{dt} > 0, \quad \frac{dY}{dt} > \frac{dZ}{dt} > 0.\tag{30}$$

Note that this coordinate system differs from the  $x, y, z$  coordinate system that is defined in section 2 and satisfies inequality 3.

As in section 2, define

$$A = \frac{dY}{dX}, \quad B = \frac{dZ}{dX}\tag{31}$$

and

$$Y_0 = Y(t)|_{X(t)=0}, \quad Z_0 = Z(t)|_{X(t)=0}. \quad (32)$$

Then

$$Y = AX + Y_0, \quad Z = BX + Z_0 \quad (33)$$

where

$$A > B > 0 \quad 0 < Y_0 < 1 \quad 0 < Z_0 < 1. \quad (34)$$

Consider the intersections of the line with the integer  $X$  coordinate planes  $\{X = n\}$ . At each intersection, the line enters a voxel that can be associated with its own coordinate system  $\{X^{(n)}, Y^{(n)}, Z^{(n)}\}$ . The entrance point of the line to the voxel in that coordinate system is

$$Y_0^{(n)} = Y_0 + An \quad Z_0^{(n)} = Z_0 + Bn. \quad (35)$$

For almost all the lines (except a zero measure set), the triplet  $\{1, A, B\}$  is linearly independent above the integers. Hence, according to Kronecker's theorem [7], for an infinite straight line, the pair  $(Y_0^{(n)}, Z_0^{(n)})$  is uniformly distributed modulo 1 in  $[0, 1)^2$ . Thus, for a randomly selected voxel  $V$  that the line passes, the entrance coordinates  $(Y_0, Z_0)$  are uniformly distributed in  $[0, 1)^2$ .

Suppose the line is digitized using Cube Quantization and represented as a 6-chain. Classify the digital line points to one of three mutually exclusive groups  $\Omega_1^{(1)}, \Omega_2^{(1)}, \Omega_3^{(1)}$  such that a point belongs to  $\Omega_m^{(1)}$  if the number of *preceding* digital line points in the 26-neighborhood of the given point is  $m$ , as shown in Fig. 2. Thus, from just outside the neighborhood the given point is reached by  $m$  chain links.

From the definition of the coordinate system it follows that each of these  $m$  chain links is necessarily in the positive direction of one of the three axes. In each direction there is a single link at most, otherwise the chain would have left the 26-neighborhood. Let  $N_X, N_Y, N_Z$  denote the number of links (0 or 1) in the  $X, Y, Z$  directions respectively. Then

$$m = N_X + N_Y + N_Z. \quad (36)$$

Since the line enters the given voxel at the  $X = 0$  face,  $N_X$  is always 1. If at the entrance point of the line to the 26-neighborhood  $Y < 0$ , there is a link in the  $Y$  direction. Since  $Y$  grows monotonically along the line, its value at the entrance point to the 26-neighborhood is

$$Y = \max\{Y|_{X=-1}, Y|_{Y=-1}, Y|_{Z=-1}\} \quad (37)$$

Thus

$$N_Y = \begin{cases} 1 & Y|_{X=-1} < 0 \quad \text{and} \quad Y|_{Z=-1} < 0 \\ 0 & \text{otherwise} \end{cases}. \quad (38)$$

Similarly,

$$N_Z = \begin{cases} 1 & Z|_{X=-1} < 0 \quad \text{and} \quad Z|_{Y=-1} < 0 \\ 0 & \text{otherwise} \end{cases}. \quad (39)$$

Substituting Eq. 33 and using inequality 34 one obtains

$$N_Y = \begin{cases} 1 & Y_0 < A \\ 0 & \text{otherwise} \end{cases} \quad (40)$$

$$N_Z = \begin{cases} 1 & Z_0 < B \quad \text{and} \quad (Y_0 + 1)B/A > Z_0 \\ 0 & \text{otherwise} \end{cases} . \quad (41)$$

The pair of slopes  $A$  and  $B$  is in one of the four following ranges:

$$\begin{aligned} \mathcal{A} : & 1 > A > B > 0 \\ \mathcal{B} : & 2 > A > 1 > B > 0 \\ \mathcal{C} : & A > 2 \quad \text{and} \quad A/2 > B > 0 \\ \mathcal{D} : & A > B > 1 \quad \text{and} \quad A/2 < B \end{aligned} \quad (42)$$

See Fig. 3a.

Figures 3b–e show  $m = 1 + N_Y + N_Z$  as a function of  $Y_0$  and  $Z_0$ , with  $A$  and  $B$  as parameters, in the four ranges  $\mathcal{A} - \mathcal{D}$  respectively. With  $(Y_0, Z_0)$  uniformly distributed, the area of a domain in which  $m = i$  represents the probability that a point in the digital line belongs to  $\Omega_i^{(1)}$ . By calculating the areas of the domains it is easy to show that the probabilities are:

$$p_1^{(1)}(A, B) = \begin{cases} (1 - A)(1 - B) & \mathcal{A} \\ 0 & \mathcal{B} \\ 0 & \mathcal{C} \\ 0 & \mathcal{D} \end{cases} \quad (43)$$

$$p_2^{(1)}(A, B) = \begin{cases} A + B - 2AB & \mathcal{A} \\ 1 - B + (A - 1)^2 B / 2A & \mathcal{B} \\ 1 - 3B / 2A & \mathcal{C} \\ A / 2B - 1 + B / 2A & \mathcal{D} \end{cases} \quad (44)$$

$$p_3^{(1)}(A, B) = \begin{cases} AB & \mathcal{A} \\ 2B - AB / 2 - B / 2A & \mathcal{B} \\ 3B / 2A & \mathcal{C} \\ 2 - A / 2B - B / 2A & \mathcal{D} \end{cases} \quad (45)$$

The  $X, Y, Z$  coordinate system is voxel-dependent (inequality 30). In order to proceed we must return to the  $x, y, z$  coordinate system. There, in the digital representation of  $l$ , the number of digital chain links in the  $x, y$  and  $z$  directions is respectively given by:

$$n_x = \frac{1}{\sqrt{1 + a^2 + b^2}} L, \quad (46)$$

$$n_y = \frac{a}{\sqrt{1 + a^2 + b^2}} L, \quad (47)$$

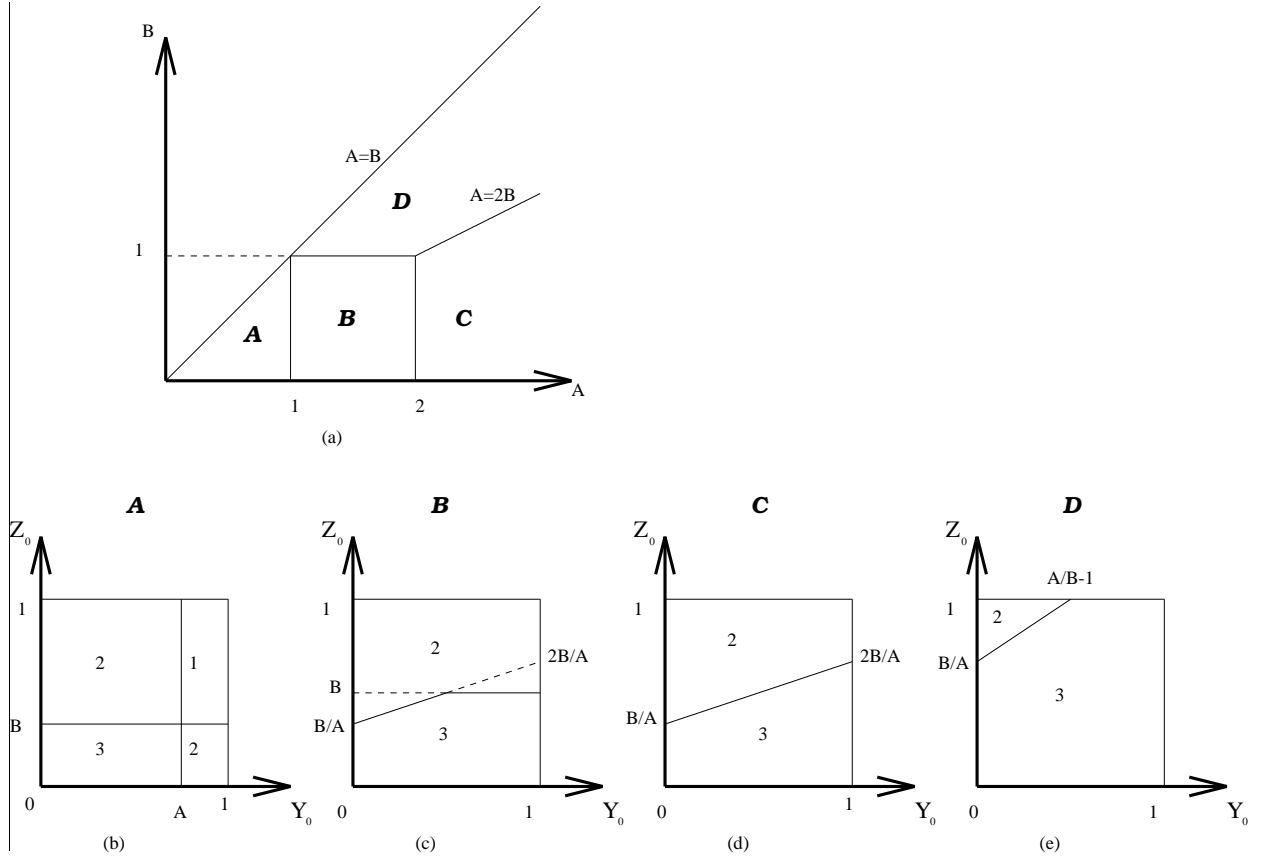


Figure 3: (a) Partition of the slopes  $(A,B)$  to four ranges. (b)–(e) The number of preceding digital line points (voxels) in the 26-neighborhood of a given digital line voxel, as a function of the entry point to the voxel  $(X_0, Y_0)$ , with  $(A,B)$  as parameters. The four graphs correspond to the four ranges shown in (a).

$$n_z = \frac{b}{\sqrt{1 + a^2 + b^2}} L. \quad (48)$$

For each voxel, the  $X, Y, Z$  coordinates correspond to a permutation of the  $(x, y, z)$  coordinates. The  $X$  axis corresponds to the the direction of the link that enters the voxel  $x, y$  or  $z$ . The axes  $Y$  and  $Z$  correspond to the remaining two axes from  $(x, y, z)$ . Since  $\frac{dY}{dt} > \frac{dZ}{dt}$  and  $\frac{dx}{dt} > \frac{dy}{dt} > \frac{dz}{dt}$ , it follows that  $Y, Z$  respectively correspond to  $x, y$  and  $z$ , after deleting the axis that corresponds to  $X$ . Thus, for voxel that is reached by an  $x$  directed link,  $X = x, Y = y, Z = z$ , following a  $y$  directed link,  $X = y, Y = x, Z = z$  and after a  $z$  directed link,  $X = z, Y = x, Z = y$ .

Having found the correspondence between the coordinate systems, the relation between the slopes  $(A, B)$  in the  $(X, Y, Z)$  system and the slopes  $(a, b)$  in the  $(x, y, z)$  system can be found.

Following a link at  $x$  direction:  $A = a$ ,  $B = b$ , following a link at  $y$  direction:  $A = 1/a$ ,  $B = b/a$  and after a link at  $z$  direction:  $A = 1/b$ ,  $B = a/b$ . Substituting each of these relations in the expressions for the class probabilities (Eqs. 43,44 and 45), respectively gives the class probabilities for voxels that have been reached by  $x$ ,  $y$  and  $z$  links. Multiplication by the number of links in each direction (Eqs. 46,47 and 48), yields the number of points that belong to  $\Omega_1^{(1)}$ ,  $\Omega_2^{(1)}$  and  $\Omega_3^{(1)}$ :

$$N_i^{(1)}(a, b) = p_i^{(1)}(a, b)n_x(a, b) + p_i^{(1)}\left(\frac{1}{a}, \frac{b}{a}\right)n_y(a, b) + p_i^{(1)}\left(\frac{1}{b}, \frac{a}{b}\right)n_z(a, b), \quad i = 1, 2, 3 \quad (49)$$

This expression can be substituted in Eqs. 10, 15 and 24 to obtain the system of equations (25). Its solution leads to the one-sided estimator, in the form of Eq. 8. The calculations, including numerical integration and solution of system of linear equations, were performed using the *Mathematica* software system. The result is:

$$\hat{L} = 0.89710N_1^{(1)} + 0.65485N_2^{(1)} + 0.54218N_3^{(1)} \quad (50)$$

The RMS error of the estimator is found, using (17) and taking the square root, to be 2.49%.

## 6 Two-sided Estimator

The one-sided estimator classifies a digital curve point according to the number of preceding digital curve points in its 26-neighborhood. In this section the estimation accuracy is improved by refinement of the classification, in particular by taking into account the number of *succeeding* digital curve points in the 26-neighborhood as well. Let  $r$  denote the number of preceding digital curve points in the 26-neighborhood of a given point, and  $s$  the number of succeeding ones. Classify the digital curve point to one of the mutually exclusive groups  $\Omega_{rs}^{(2*)}$ . For a digital straight line  $r, s = 1, 2, 3$ , hence there are nine groups.

From the direction symmetry of cube quantization it follows that the number of points  $N_{rs}^{(2*)}$  in  $\Omega_{rs}^{(2*)}$  satisfies:

$$N_{rs}^{(2*)} = N_{sr}^{(2*)}, \quad r = 1, 2, 3, \quad s = 1, 2, 3. \quad (51)$$

For a digital line, the nine groups are related to the three groups  $\{\Omega_m^{(1)}\}$  defined in section 5:

$$\Omega_{11}^{(2*)} \cup \Omega_{12}^{(2*)} \cup \Omega_{13}^{(2*)} = \Omega_1^{(1)} \quad (52)$$

$$\Omega_{21}^{(2*)} \cup \Omega_{22}^{(2*)} \cup \Omega_{23}^{(2*)} = \Omega_2^{(1)} \quad (53)$$

$$\Omega_{31}^{(2*)} \cup \Omega_{32}^{(2*)} \cup \Omega_{33}^{(2*)} = \Omega_3^{(1)} \quad (54)$$

Since the nine groups  $\{\Omega_{rs}^{(2*)}\}$  are mutually exclusive and the three groups  $\{\Omega_m^{(1)}\}$  are mutually exclusive, a relation between the numbers of points in them follows:

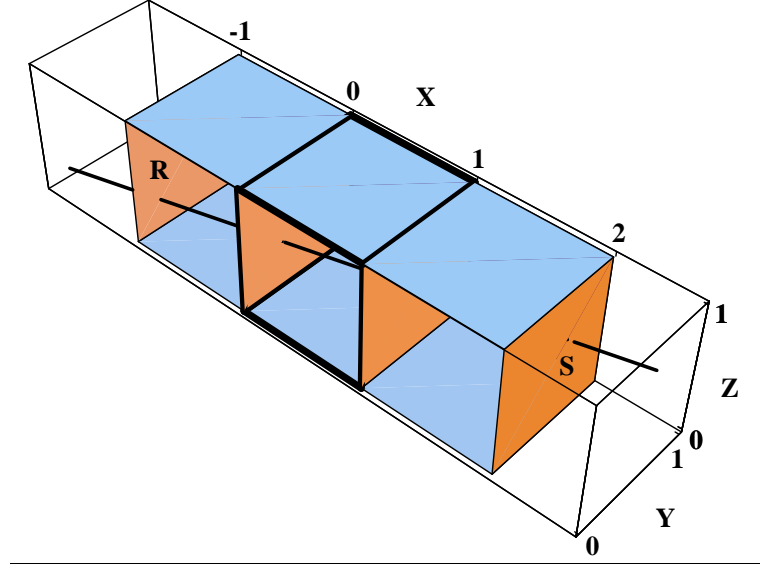


Figure 4:  $\Omega_{11}^{(2*)}$  type voxel. The highlighted voxel has two 26-neighbors, one in each side. The line enters the 26-neighborhood through face  $R$  and leaves through face  $S$ .

$$\begin{cases} N_{11}^{(2*)} + N_{12}^{(2*)} + N_{13}^{(2*)} = N_1^{(1)} \\ N_{12}^{(2*)} + N_{22}^{(2*)} + N_{23}^{(2*)} = N_2^{(1)} \\ N_{13}^{(2*)} + N_{23}^{(2*)} + N_{33}^{(2*)} = N_3^{(1)} \end{cases} \quad (55)$$

This is a system of three equations with six unknowns. Once three of the unknowns are independently determined, the rest can be found using Eqs. 55.

We first find  $N_{11}^{(2*)}$ , using the coordinate system  $(X, Y, Z)$  defined in section 5. A voxel in  $\Omega_{11}^{(2*)}$  is illustrated in figure 4. It is clear that in this configuration the line always enters one neighbor in the face marked  $R$  and leaves another neighbor from the face marked  $S$ . Formally,

$$\begin{cases} 0 < Y|_{X=-1} < 1 \\ 0 < Z|_{X=-1} < 1 \\ 0 < Y|_{X=2} < 1 \\ 0 < Z|_{X=2} < 1 \end{cases} \quad (56)$$

Substituting Eq. 33 leads to:

$$\begin{cases} 0 < Y_0 - A < 1 \\ 0 < Z_0 - B < 1 \\ 0 < Y_0 + 2A < 1 \\ 0 < Z_0 + 2B < 1 \end{cases} \quad (57)$$

or, in short,

$$\begin{cases} A < Y_0 < 1 - 2A \\ B < Z_0 < 1 - 2B \end{cases} \quad (58)$$

As explained in section 5,  $(Y_0, Z_0)$  are uniformly distributed above  $[0, 1]^2$ , hence the probability of a point to be in  $\Omega_{11}^{(2*)}$  is:

$$p_{11}^{(2*)}(A, B) = \begin{cases} (1 - 3A)(1 - 3B) & \frac{1}{3} > A > B \\ 0 & \text{otherwise} \end{cases} \quad (59)$$

We found  $p_{11}^{(2*)}(A, B)$ . Similar to Eq. (49), in the  $(x, y, z)$  coordinate system, in terms of the slopes  $(a, b)$ , the total number of elements  $N_{11}^{(2*)}(a, b)$  is

$$N_{11}^{(2*)}(a, b) = p_{11}^{(2*)}(a, b)n_x(a, b) + p_{11}^{(2*)}\left(\frac{1}{a}, \frac{b}{a}\right)n_y(a, b) + p_{11}^{(2*)}\left(\frac{1}{b}, \frac{a}{b}\right)n_z(a, b). \quad (60)$$

We proceed to find  $N_{21}^{(2*)}$ , the number of elements in  $\Omega_{21}^{(2*)}$ . There are four possible cases, shown in Fig. 5, defined by the following sets of conditions:

$$\begin{array}{cc} \begin{array}{l} a \\ \left\{ \begin{array}{l} 0 < Y|_{X=-1} < 1 \\ -1 < Z|_{X=-1} < 0 \\ 0 < Y|_{X=2} < 1 \\ 0 < Z|_{X=2} < 1 \end{array} \right. \end{array} & \begin{array}{l} b \\ \left\{ \begin{array}{l} -1 < Y|_{X=-1} < 0 \\ 0 < Z|_{X=-1} < 1 \\ 0 < Y|_{X=2} < 1 \\ 0 < Z|_{X=2} < 1 \end{array} \right. \end{array} \\ \begin{array}{l} c \\ \left\{ \begin{array}{l} -1 < Y|_{X=-1} < 0 \\ 0 < Z|_{X=-1} < 1 \\ 0 < X|_{Y=2} < 1 \\ 0 < Z|_{Y=2} < 1 \end{array} \right. \end{array} & \begin{array}{l} d \\ \left\{ \begin{array}{l} -1 < X|_{Y=-1} < 0 \\ 0 < Z|_{Y=-1} < 1 \\ 0 < X|_{Y=2} < 1 \\ 0 < Z|_{Y=2} < 1 \end{array} \right. \end{array} \end{array} \quad (61)$$

Substituting (33) we obtain:

$$\begin{array}{cc} \begin{array}{l} a \\ \left\{ \begin{array}{l} 0 < Y_0 - A < 1 \\ -1 < Z_0 - B < 0 \\ 0 < Y_0 + 2A < 1 \\ 0 < Z_0 + 2B < 1 \end{array} \right. \end{array} & \begin{array}{l} b \\ \left\{ \begin{array}{l} -1 < Y_0 - A < 0 \\ 0 < Z_0 - B < 1 \\ 0 < Y_0 + 2A < 1 \\ 0 < Z_0 + 2B < 1 \end{array} \right. \end{array} \\ \begin{array}{l} c \\ \left\{ \begin{array}{l} -1 < Y_0 - A < 0 \\ 0 < Z_0 - B < 1 \\ 0 < (2 - Y_0)/A < 1 \\ 0 < Z_0 + (2 - Y_0)B/A < 1 \end{array} \right. \end{array} & \begin{array}{l} d \\ \left\{ \begin{array}{l} -1 < -(Y_0 + 1)/A < 0 \\ 0 < Z_0 - (Y_0 + 1)B/A < 1 \\ 0 < (2 - Y_0)/A < 1 \\ 0 < Z_0 + (2 - Y_0)B/A < 1 \end{array} \right. \end{array} \end{array} \quad (62)$$

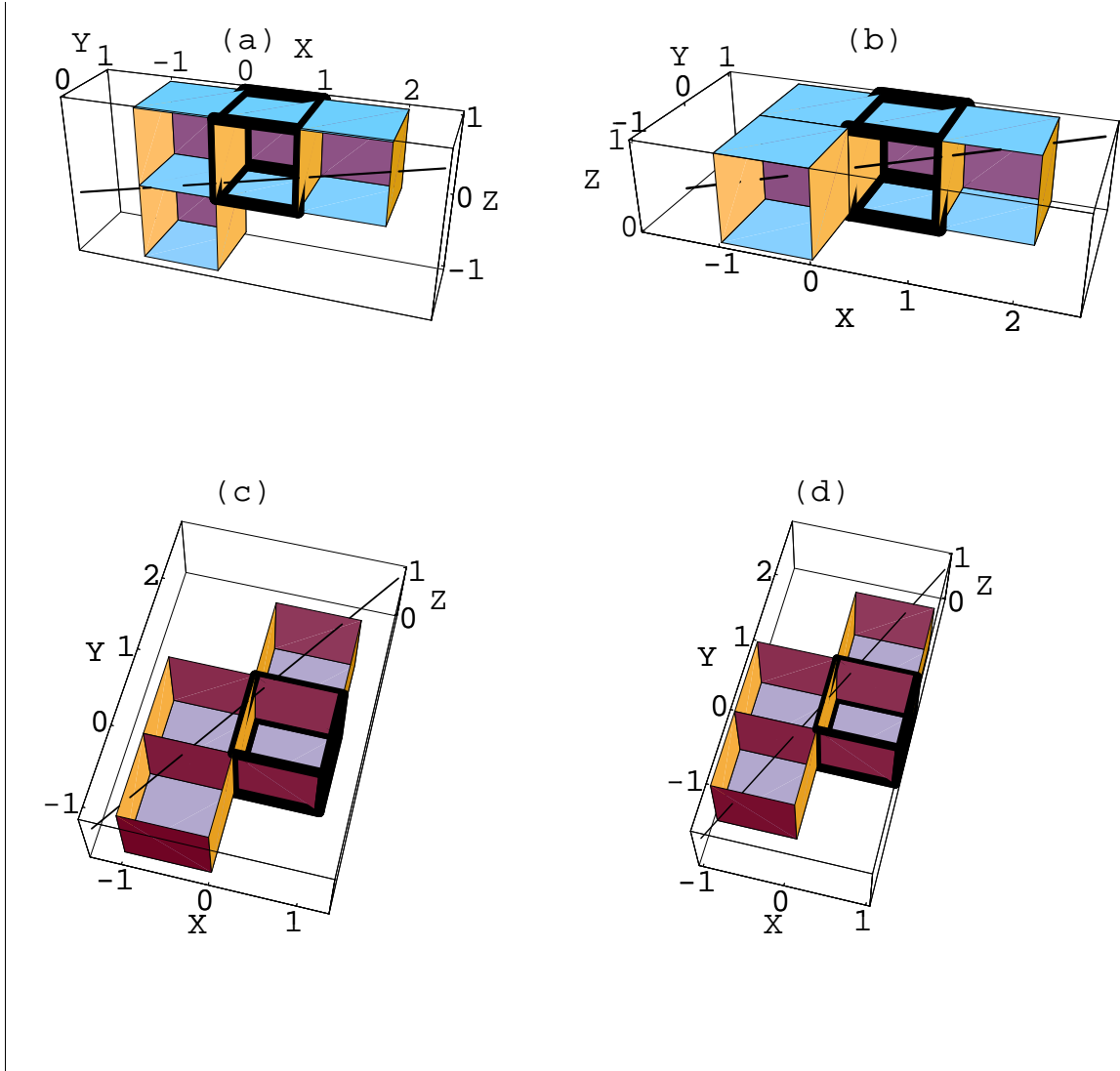


Figure 5: Four possible cases of  $\Omega_{21}^{(2*)}$  voxels. In all the cases, the highlighted voxel has two preceding 26-neighbors and one succeeding 26-neighbor. The differences are in the faces through which the line enters and leaves the 26-neighborhood of the voxel.

The pair of slopes  $(A, B)$  is in one of the following seven ranges, shown in Figure 6a.

$$\begin{aligned}
\mathcal{A} : & 1/3 > A > B \\
\mathcal{B} : & 1/2 > A > 1/3 > B \\
\mathcal{C} : & 3/2 > A > 1, 1/2 > B \\
\mathcal{D} : & 2 > A > 3/2, A/3 > B \\
\mathcal{E} : & 2 > A > 1, \frac{A}{A+1} > B > \max\{1, \frac{A}{3}\} \\
\mathcal{F} : & A > 2, A/3 > B \\
\mathcal{G} : & \text{otherwise}
\end{aligned} \tag{63}$$

Figures 6b–i show the domains of  $(Y_0, Z_0)$  that correspond to inequalities 62 with  $A$  and  $B$  as parameters. The results depend on the range.

The probability of each of the four cases is obtained by calculating the respective areas:

$$p_{21a}^{(2*)}(A, B) = \begin{cases} (1 - 3A)B & 1/3 > A > B \\ 0 & \text{otherwise} \end{cases} \tag{64}$$

$$p_{21b}^{(2*)}(A, B) = \begin{cases} (1 - 3B)A & 1/3 > A > B \\ (1 - 2A)(1 - 3B) & 1/2 > A > 1/3 > B \\ 0 & \text{otherwise} \end{cases} \tag{65}$$

$$p_{21c}^{(2*)}(A, B) = \begin{cases} (A - 1)(1 - 3B/2 - B/2A) & 3/2 > A > 1, 1/2 > B \\ (A - B - AB)^2/2AB & 2 > A > 3/2, A/3 > B \\ (A - B - AB)^2/2AB & 2 > A > 1, \frac{A}{A+1} > B > \max\{1, \frac{A}{3}\} \\ 0 & \text{otherwise} \end{cases} \tag{66}$$

$$p_{21d}^{(2*)}(A, B) = \begin{cases} (1 - 3B/A)(2A - 3) & 2 > A > 3/2, A/3 > B \\ 1 - 3B/A & A > 2, A/3 > B \\ 0 & \text{otherwise} \end{cases} \tag{67}$$

Summing the probabilities of the four cases gives the probability of a point to be in  $\Omega_{21}^{(2*)}$ :

$$p_{21}^{(2*)}(A, B) = \begin{cases} A + B - 6AB & 1/3 > A > B \\ (1 - 2A)(1 - 3B) & 1/2 > A > 1/3 > B \\ (A - 1)(1 - 3B/2 - B/2A) & 3/2 > A > 1, 1/2 > B \\ A + AB/2 + 5B/A - 5B - 1 & 2 > A > 3/2, A/3 > B \\ (A - B - AB)^2/2AB & 2 > A > 1, \frac{A}{A+1} > B > \max\{1, \frac{A}{3}\} \\ 1 - 3B/A & A > 2, A/3 > B \\ 0 & \text{otherwise} \end{cases} \tag{68}$$

We found  $p_{21}^{(2*)}(A, B)$ . Similar to Eq. (60), in the  $(x, y, z)$  coordinate system, in terms of the slopes  $(a, b)$ , the total number of elements  $N_{11}^{(2*)}(a, b)$  is

$$N_{21}^{(2*)}(a, b) = p_{21}^{(2*)}(a, b)n_x(a, b) + p_{21}^{(2*)}\left(\frac{1}{a}, \frac{b}{a}\right)n_y(a, b) + p_{21}^{(2*)}\left(\frac{1}{b}, \frac{a}{b}\right)n_z(a, b). \tag{69}$$

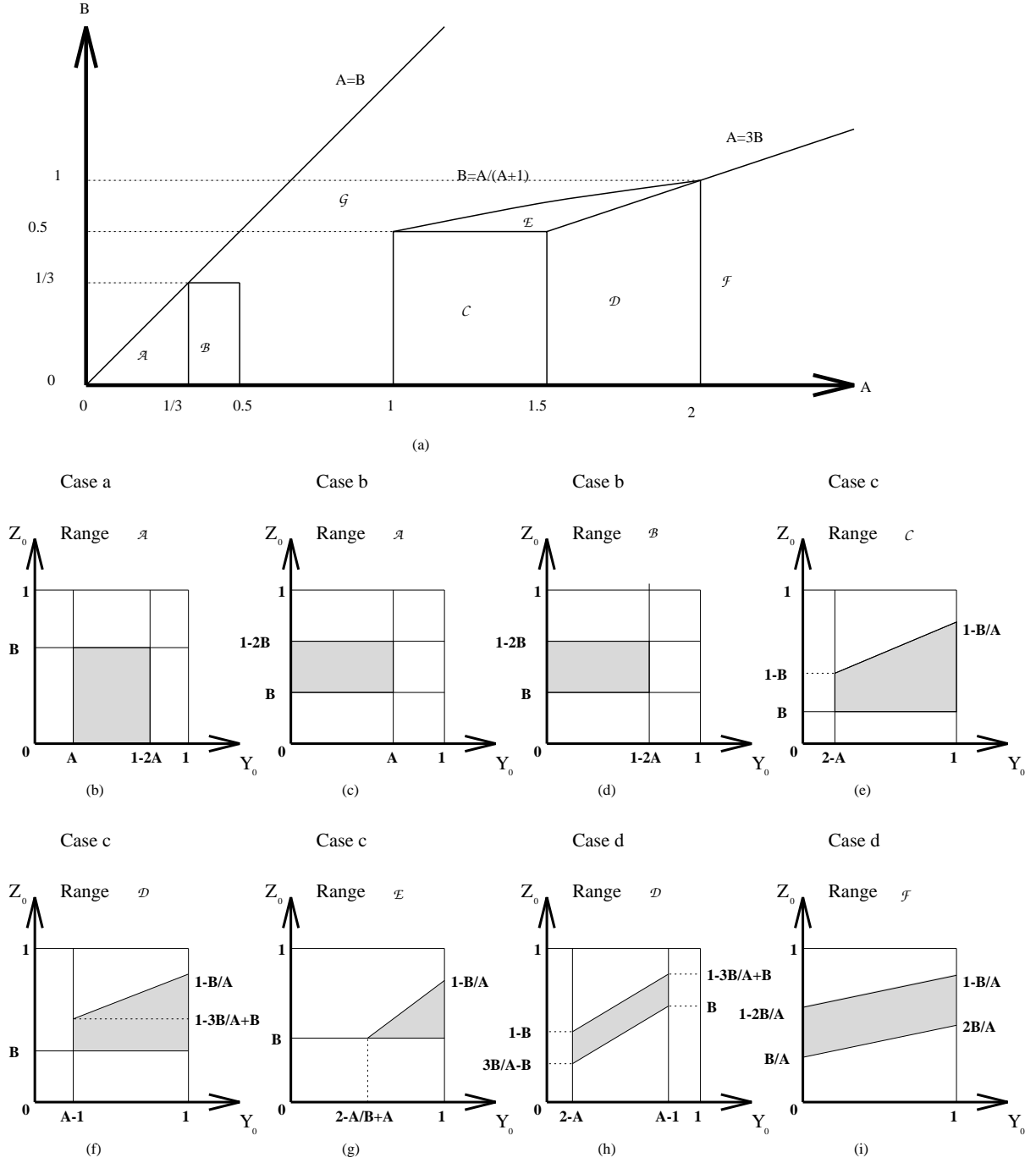


Figure 6: Conditions on straight lines for a given voxel to be of type  $\Omega_{21}^{(2*)}$ . (a) Partition of the slopes  $(A,B)$  to seven ranges. (b)–(i) The domains of  $(Y_0, Z_0)$  that lead to the the four cases of  $\Omega_{21}^{(2*)}$  voxels (figure 5) are shown with  $(A, B)$  as parameters, and in reference to the seven ranges shown in (a). Only combinations that lead to  $\Omega_{21}^{(2*)}$  voxels are shown.

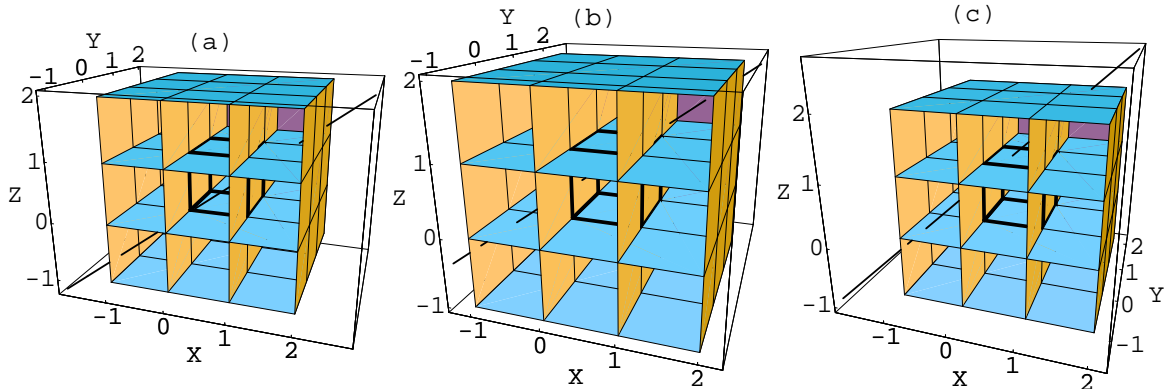


Figure 7: Three types of voxels in  $\Omega_{33}^{(2*)}$  (highlighted, and shown with their 26-neighborhood). The coordinate system axes are set such that the entry point to the 26-neighborhood is always in the  $X = -1$  plane. The three types correspond to three faces through which the line exits the 26-neighborhood.

For the calculation of  $N_{33}^{(2*)}$ , the number of voxels in  $\Omega_{33}^{(2*)}$ , we observe that a voxel centered at  $(x, y, z)$  is in the chain and belongs to  $\Omega_{33}^{(2*)}$  if and only if  $(x - 1, y - 1, z - 1)$  and  $(x + 1, y + 1, z + 1)$  are in the chain. Hence, the number of the chain points in  $\Omega_{33}^{(2*)}$  can be found by counting the number of pairs of the form  $(x, y, z)$  and  $(x + 2, y + 2, z + 2)$  in the chain. Consider in turn a voxel through which the line passes. Use that voxel to define the  $(X, Y, Z)$  coordinate system as in section 5. Now, one has to check whether that voxel is the first in a pair of voxels in the chain that differ by 2 in each of their coordinates. If that is the case, then there is a voxel located at  $(x + 1, y + 1, z + 1)$  between them along the chain, that is in  $\Omega_{33}^{(2*)}$ .

There are three possible ways for a line to pass through the said pair of voxels, defined according to the face through which the line leaves the second voxel of the pair, as shown in Fig. 7. The three cases, formally defined by the following inequalities, correspond to three types of voxels in  $\Omega_{33}^{(2*)}$ .

$$\begin{array}{ccc}
 a & b & c \\
 \left\{ \begin{array}{l} 2 < Y|_{X=3} < 3 \\ 2 < Z|_{X=3} < 3 \end{array} \right. & \left\{ \begin{array}{l} 2 < X|_{Y=3} < 3 \\ 2 < Z|_{Y=3} < 3 \end{array} \right. & \left\{ \begin{array}{l} 2 < X|_{Z=3} < 3 \\ 2 < Y|_{Z=3} < 3 \end{array} \right. \quad . \quad (70)
 \end{array}$$

Substituting Eqs. 33 we obtain:

$$\begin{array}{l}
a \\
\left\{ \begin{array}{l} 2 - 3A < Y_0 < 3 - 3A \\ 2 - 3B < Z_0 < 3 - 3B \end{array} \right. \\
b \\
\left\{ \begin{array}{l} 3 - 3A < Y_0 < 3 - 2A \\ 2 - (3 - Y_0)B/A < Z_0 < 3 - (3 - Y_0)B/A \end{array} \right. \\
c \\
\left\{ \begin{array}{l} 3 - 3B < Z_0 < 3 - 2B \\ 2 - (3 - Z_0)A/B < Y_0 < 3 - (3 - Z_0)A/B \end{array} \right.
\end{array} \quad . \quad (71)$$

The pair of slopes  $(A, B)$  is in one of the following nine ranges, shown in Figure 8.

$$\begin{array}{l}
\mathcal{A} \quad \frac{1}{3} < A < \frac{2}{3} \quad \text{and} \quad \frac{1}{3} < B < A \\
\mathcal{B} \quad \frac{2}{3} < A < 1 \quad \text{and} \quad \frac{1}{3} < B < \frac{A}{2} \\
\mathcal{C} \quad \frac{A}{2} < B < \frac{2}{3} < A < 1 \\
\mathcal{D} \quad \frac{2}{3} < A < 1 \quad \text{and} \quad \frac{2}{3} < B < A \\
\mathcal{E} \quad 1 < A < \frac{3}{2} \quad \text{and} \quad \frac{A}{3} < B < \frac{1}{2} \\
\mathcal{F} \quad 1 < A < \frac{3}{2} \quad \text{and} \quad \frac{1}{2} < B < \frac{2A}{3} \\
\mathcal{G} \quad \frac{2A}{3} < B < 1 < A < \frac{3}{2} \\
\mathcal{H} \quad 1 < A < \frac{3}{2} \quad \text{and} \quad 1 < B < A \\
\mathcal{I} \quad \text{otherwise}
\end{array} \quad . \quad (72)$$

Fig. 9 shows the domains of  $(Y_0, Z_0)$  that correspond to these inequalities, with  $A$  and  $B$  as parameters. The results depend on the range.

The probability of each of the cases is obtained by calculating the respective areas.

$$p_{33a}^{(2*)}(A, B) = \begin{cases} (3A - 1)(3B - 1) & \frac{1}{3} < A < \frac{2}{3} \quad \text{and} \quad \frac{1}{3} < B < A \\ (3 - 3A)(3B - 1) & \frac{1}{3} < B < \frac{2}{3} < A < 1 \\ (3 - 3A)(3 - 3B) & \frac{2}{3} < A < 1 \quad \text{and} \quad \frac{2}{3} < B < A \\ 0 & \text{otherwise} \end{cases} \quad . \quad (73)$$

$$p_{33b}^{(2*)}(A, B) = \begin{cases} \frac{1}{2}(3B - 1)A(3 - \frac{1}{B}) & \frac{2}{3} < A < 1 \quad \text{and} \quad \frac{1}{3} < B < \frac{A}{2} \\ (3A - 2)[B(\frac{3}{2} + \frac{1}{A}) - 1] & \frac{A}{2} < B < \frac{2}{3} < A < 1 \\ 2 + 9A - \frac{9}{2}AB - \frac{4A}{B} - \frac{2B}{A} & \frac{2}{3} < A < 1 \quad \text{and} \quad \frac{2}{3} < B < A \\ \frac{1}{2}(3 - \frac{A}{B})(\frac{3B}{A} - 1) & 1 < A < \frac{3}{2} \quad \text{and} \quad \frac{A}{3} < B < \frac{1}{2} \\ (3 - 2A)[B(\frac{3}{2A} + 1) - 1] & 1 < A < \frac{3}{2} \quad \text{and} \quad \frac{1}{2} < B < \frac{2A}{3} \\ 9 + 2A - \frac{4A}{B} - \frac{9B}{2A} - 2AB & \frac{2A}{3} < B < 1 < A < \frac{3}{2} \\ (3 - 2A)(3 - B - \frac{3B}{2A}) & 1 < A < \frac{3}{2} \quad \text{and} \quad 1 < B < A \\ 0 & \text{otherwise} \end{cases} \quad . \quad (74)$$

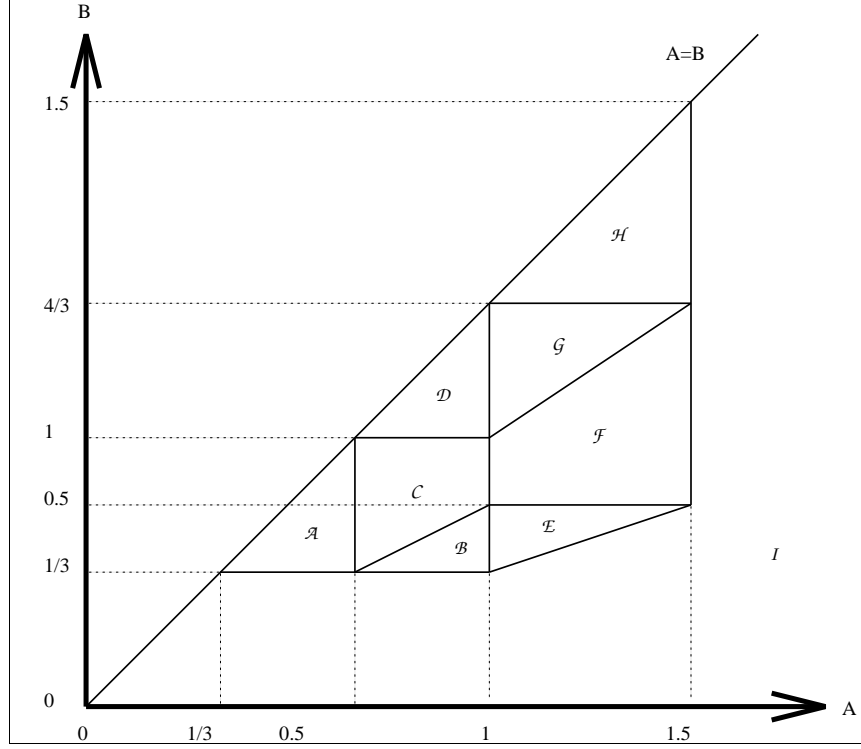


Figure 8: Partition of the slopes (A,B) to nine ranges.

$$p_{33c}^{(2*)}(A, B) = \begin{cases} (3 - 2A)(3 - B - \frac{3B}{2A}) & \frac{2}{3} < A < 1 \quad \text{and} \quad \frac{2}{3} < B < A \\ \frac{1}{2}(3 - \frac{2A}{B})(\frac{3B}{A} - 2) & \frac{2A}{3} < B < 1 < A < \frac{3}{2} \\ \frac{1}{2}(3 - 2A)(\frac{3B}{A} - 2B) & 1 < A < \frac{3}{2} \quad \text{and} \quad 1 < B < A \\ 0 & \text{otherwise} \end{cases} \quad (75)$$

Summing the probabilities of the three cases gives the probability of a point to be in  $\Omega_{33}^{(2*)}$ :

$$p_{33}^{(2*)}(A, B) = \begin{cases} (3A - 1)(3B - 1) & \frac{1}{3} < A < \frac{2}{3} \quad \& \quad \frac{1}{3} < B < A \\ \frac{1}{2}(3B - 1)A(3 - \frac{1}{B}) + (3 - 3A)(3B - 1) & \frac{2}{3} < A < 1 \quad \& \quad \frac{1}{3} < B < \frac{A}{2} \\ (3 - 3A)(3B - 1) + (3A - 2)[B(\frac{3}{2} + \frac{1}{A}) - 1] & \frac{A}{2} < B < \frac{2}{3} < A < 1 \\ 5 - \frac{2A}{B} - \frac{2B}{A} & \frac{2}{3} < A < 1 \quad \& \quad \frac{2}{3} < B < A \\ \frac{1}{2}(3 - \frac{A}{B})(\frac{3B}{A} - 1) & 1 < A < \frac{3}{2} \quad \& \quad \frac{A}{3} < B < \frac{1}{2} \\ (3 - 2A)[B(\frac{3}{2A} + 1) - 1] & 1 < A < \frac{3}{2} \quad \& \quad \frac{1}{2} < B < \frac{2A}{3} \\ 3 + 2A - \frac{2A}{B} - 2AB & \frac{2A}{3} < B < 1 < A < \frac{3}{2} \\ (3 - 2A)(3 - B - \frac{3B}{2A}) + \frac{1}{2}(3 - 2A)(\frac{3B}{A} - 2B) & 1 < A < \frac{3}{2} \quad \& \quad 1 < B < A \\ 0 & \text{otherwise} \end{cases} \quad (76)$$

We found  $p_{33}^{(2*)}(A, B)$ . Similar to Eq. (60), in the  $(x, y, z)$  coordinate system, in terms of

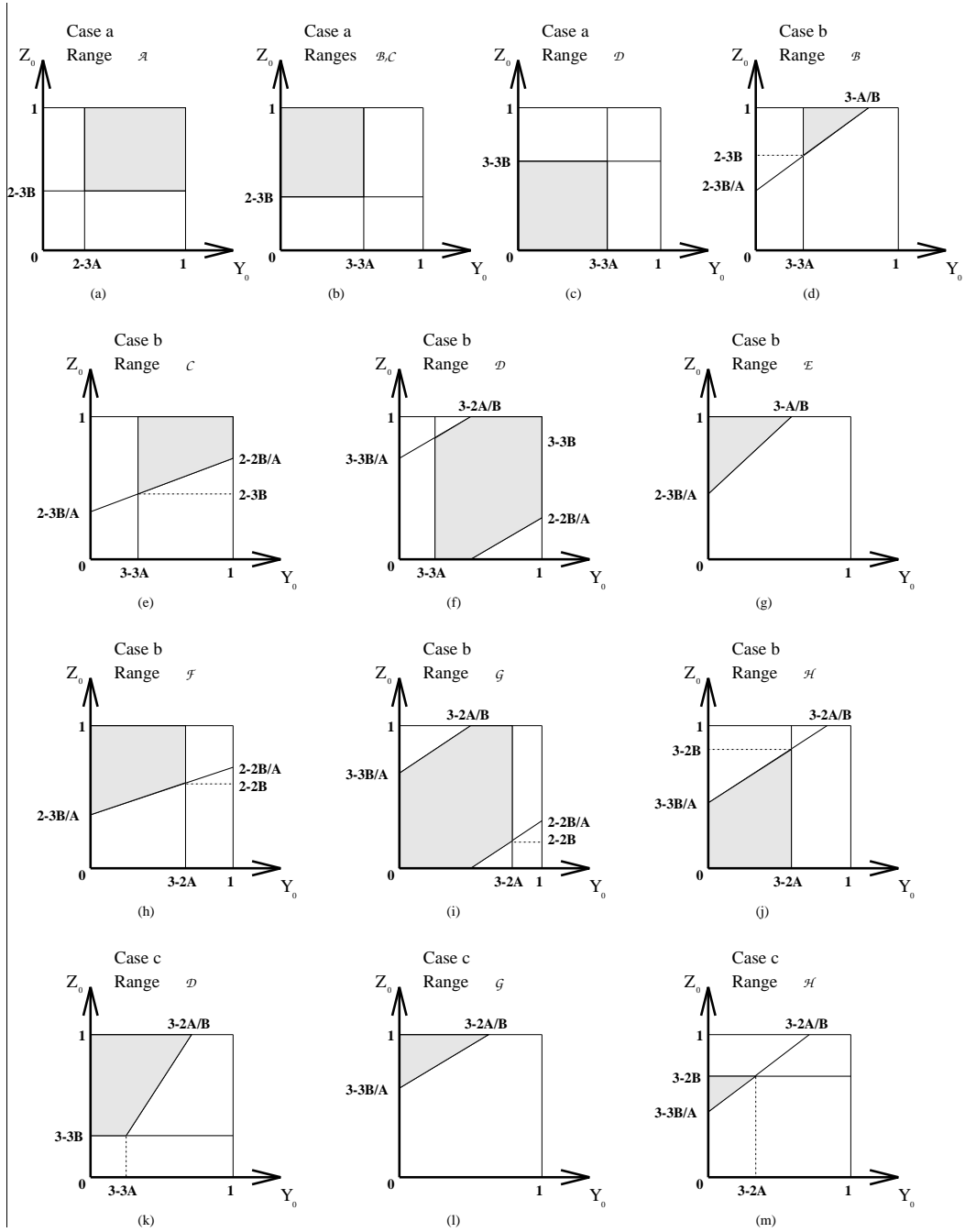


Figure 9: Conditions on straight lines for a given voxel to be of an  $\Omega_{33}^{(2*)}$  type. For each of the three cases for getting  $\Omega_{33}^{(2*)}$  type voxel (figure 7) and the different slope ranges (figure 8), all the line entry points to the voxel that lead to that case, are shown in grey. Only the possible combinations are shown. For the other combinations, the specific case is impossible for any line in the given slopes range.

the slopes  $(a, b)$ , the total number of elements  $N_{33}^{(2*)}(a, b)$  is

$$N_{33}^{(2*)}(a, b) = p_{33}^{(2*)}(a, b)n_x(a, b) + p_{33}^{(2*)}\left(\frac{1}{a}, \frac{b}{a}\right)n_y(a, b) + p_{33}^{(2*)}\left(\frac{1}{b}, \frac{a}{b}\right)n_z(a, b). \quad (77)$$

The total number of the elements of the other types  $N_{rs}^{(2*)}$  can be found using Eqs. (51) and (55):

$$\begin{aligned} N_{12}^{(2*)} &= N_{21}^{(2*)} \\ N_{13}^{(2*)} &= N_{31}^{(2*)} = N_1^{(1)} - N_{11}^{(2*)} - N_{12}^{(2*)} \\ N_{23}^{(2*)} &= N_{32}^{(2*)} = N_3^{(1)} - N_{13}^{(2*)} - N_{33}^{(2*)} \\ N_{22}^{(2*)} &= N_2^{(1)} - N_{12}^{(2*)} - N_{23}^{(2*)} \end{aligned} \quad (78)$$

Since  $N_{rs}^{(2*)} = N_{sr}^{(2*)}$ , similar symmetry will appear in the estimator coefficients too, so  $\Psi_{rs}$  and  $\Psi_{sr}$  will be equal. Since distinction between the groups  $\Omega_{rs}^{(2*)}$  and  $\Omega_{sr}^{(2*)}$  is not needed, they can be unified to obtain the following new classification groups:

$$\Omega_{rs}^{(2)} = \begin{cases} \Omega_{rs}^{(2*)} \cup \Omega_{sr}^{(2*)} & r < s \\ \Omega_{rs}^{(2*)} & r = s \end{cases}. \quad (79)$$

The numbers of elements in these groups are:

$$N_{rs}^{(2)} = \begin{cases} 2N_{rs}^{(2*)} & r < s \\ N_{rs}^{(2*)} & r = s \end{cases}. \quad (80)$$

These values can be substituted in Eqs. 10, 15 and 24 to obtain the system of equations (25). Its solution leads to the desired two-sided estimator, in the form of Eq. 8. The calculations, including numerical integration and solution of system of linear equations, were performed using the *Mathematica* software system. The result is:

$$\hat{L}_2 = 0.98817N_{11}^{(2)} + 0.77296N_{12}^{(2)} + 0.62154N_{13}^{(2)} + 0.69037N_{22}^{(2)} + 0.60158N_{23}^{(2)} + 0.56782N_{33}^{(2)} \quad (81)$$

The RMS error of the estimator is found, using (17) and taking the square root, to be 0.57%.

We have thus obtained an estimator that is based on classification of the digital curve points according to the number of their preceding and succeeding 26-neighbors. The resulting precision is much better than in all previously available estimators, including the one sided estimator.

## 7 Direct Length Estimation from the Binary Image

The length estimators that have been suggested in the literature for curves in two and three dimensions, as well as the one and two sided estimators, rely on chain code representation of the input curves. It is thus required to explicitly keep track of the order of voxels along the curve. The following estimator does not rely on order and thus can thus operate directly on the digital image and eliminate the need for prior chain code representation.

In this estimator, classification is based on the groups  $\Omega_m^{(3)}$  defined such that a digital curve voxel is in  $\Omega_m^{(3)}$  if there are exactly  $m$  digital curve voxels in its 26-neighborhood. For smooth curves without digital self intersections, and in particular for digital straight lines, the following relations to the classification groups  $\Omega_{rs}^{(2)}$  that are used in the two sided length estimator hold:

$$\begin{aligned}\Omega_2^{(3)} &= \Omega_{11}^{(2)} \\ \Omega_3^{(3)} &= \Omega_{12}^{(2)} \\ \Omega_4^{(3)} &= \Omega_{13}^{(2)} \cup \Omega_{22}^{(2)} \\ \Omega_5^{(3)} &= \Omega_{23}^{(2)} \\ \Omega_6^{(3)} &= \Omega_{33}^{(2)}\end{aligned}\tag{82}$$

The relations between the respective cardinalities are

$$\begin{aligned}N_2^{(3)} &= N_{11}^{(2)} \\ N_3^{(3)} &= N_{12}^{(2)} \\ N_4^{(3)} &= N_{13}^{(2)} + N_{22}^{(2)} \\ N_5^{(3)} &= N_{23}^{(2)} \\ N_6^{(3)} &= N_{33}^{(2)}\end{aligned}\tag{83}$$

These values can be substituted in Eqs. 10, 15 and 24 to obtain the system of equations (25). Its solution leads to the following estimator:

$$\hat{L}_3 = 0.98111N_2^{(3)} + 0.77539N_3^{(3)} + 0.66483N_4^{(3)} + 0.60050N_5^{(3)} + 0.56479N_6^{(3)}\tag{84}$$

The RMS error for uniformly distributed straight lines is 1.13%, twice than that of the two-sided estimator, but significantly superior to that of any other previously available estimator. Voxel ordering information is not required and direct operation on the 3-D digital image is possible. Note however that since it is assumed that the ordering of the digital curve voxels is unknown, then if the curve intersects itself (or is close to that), the contribution of voxels near the intersection to the length estimate will be biased.

## 8 Experiments

The suggested length estimators are designed to be unbiased and to minimize the mean square error for straight lines of random orientations. When operated on general curves with varying tangent orientations, local length estimation errors tend to cancel out, hence the total estimation error is usually greatly reduced.

In order to corroborate the analytic results the suggested estimators have been operated on 100 straight lines of length 1000 and random orientation that have been generated and digitized by computer simulation. The results are summarized in Table 2. The very small mean errors reflect the unbiasedness of the estimators. The experimental RMS errors are quite close to the values obtained by analysis. The experimental minimum, maximum and mean absolute errors are also shown.

In order to evaluate the performance of the three suggested length estimators on curves other than straight lines, experiments in length estimation of circles have been carried out. On one hand, at large radii, these experiments are intended to demonstrate that local estimation errors tend to cancel out in curves with varying tangent orientations. On the other hand, at small radii, they allow to observe the performance degradation as curvature increases and the assumption that curves are smooth almost everywhere becomes less and less valid.

In the following graphs, the value at each radius is based on length estimation of 100 circles at random locations and orientations that have been generated and digitized by computer simulation. Fig. 10 shows the maximal, average and minimal perimeter estimation errors over that set of circles using the one-sided length estimator. Figs. 11 and 12 respectively refer to the two-sided and direct length estimators. Fig. 13 compares the RMS estimation errors of the three estimators. The corresponding average absolute errors are compared in Fig. 14.

Estimator	mean err.	RMS err.	min err.	max. err.	mean abs. err.
$\hat{L}_1$ (1-sided)	-0.04%	2.52%	-7.46%	4.07%	1.94%
$\hat{L}_2$ (2-sided)	-0.09%	0.61%	-1.60%	1.02%	0.49%
$\hat{L}_3$ (direct)	-0.09%	1.27%	-4.61%	1.46%	0.87%

Table 2: Length estimation of 100 straight lines of length 1000 and random orientation using the three estimators presented in this paper. Shown are the mean, RMS, minimum, maximum, and mean absolute length estimation errors.

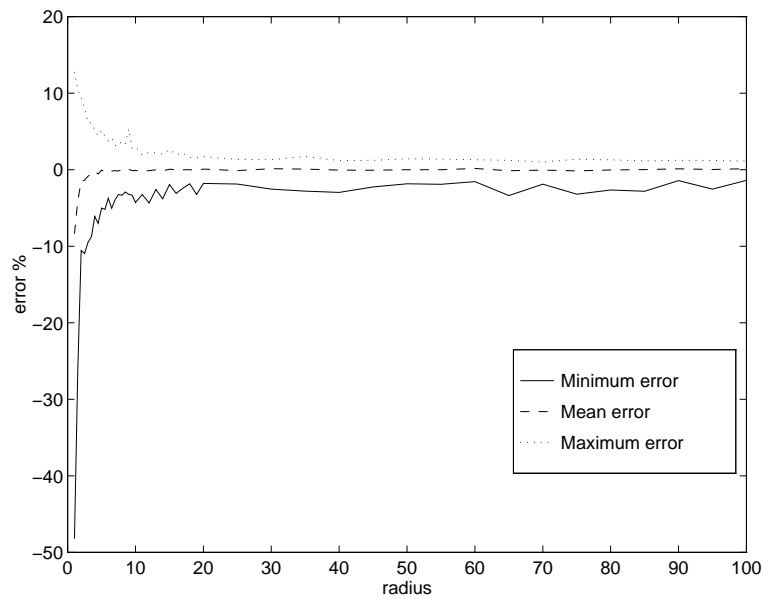


Figure 10: Perimeter estimation of circles using the one sided estimator. For each radius, the maximum, minimum and average errors over a set of 100 random circles are presented.

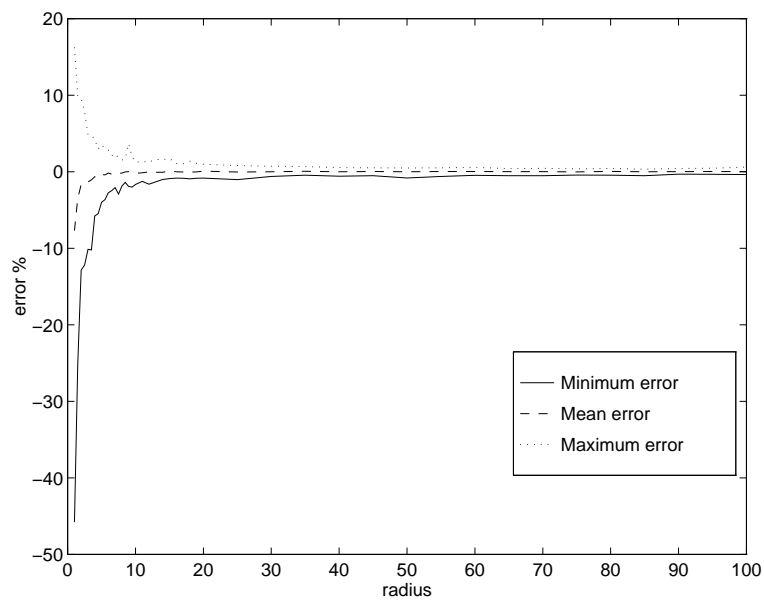


Figure 11: Perimeter estimation of circles using the two sided estimator. For each radius, the maximum, minimum and average errors over a set of 100 random circles are presented.

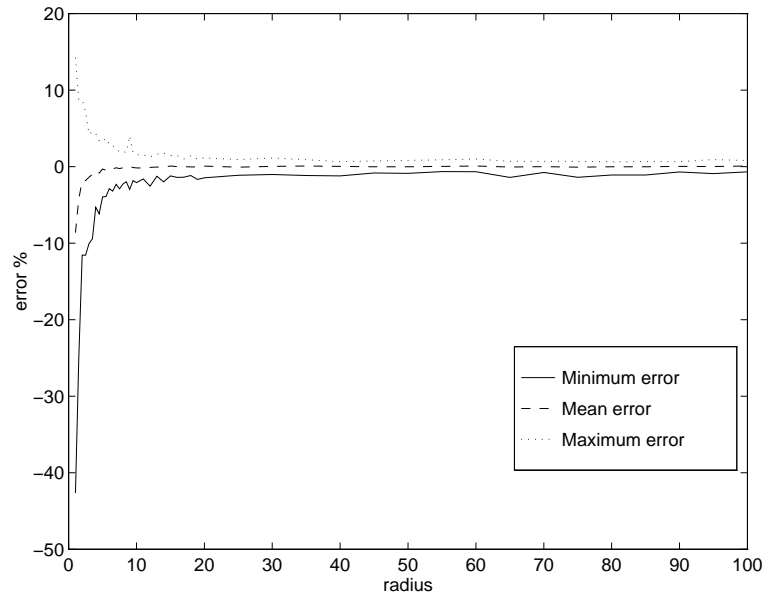


Figure 12: Perimeter estimation of circles using the direct estimator. For each radius, the maximum, minimum and average errors over a set of 100 random circles are presented.

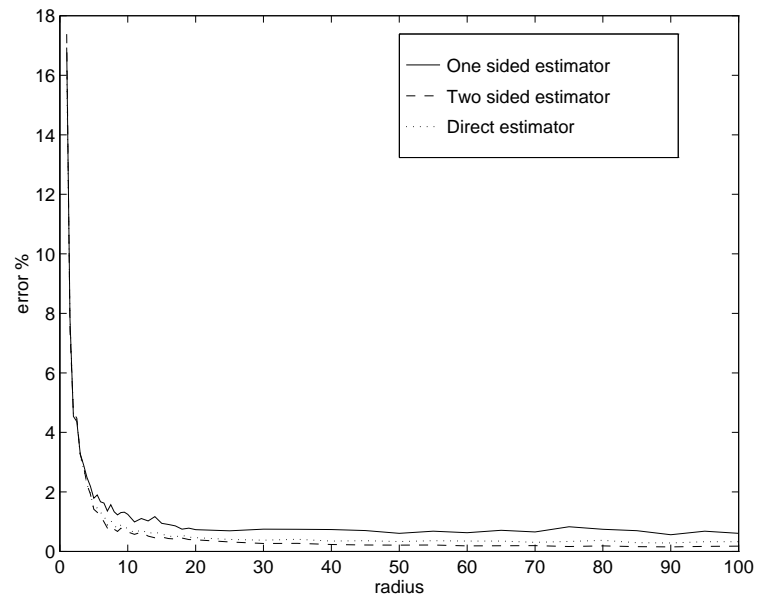


Figure 13: The RMS errors in perimeter estimation of circles using the three suggested estimators.

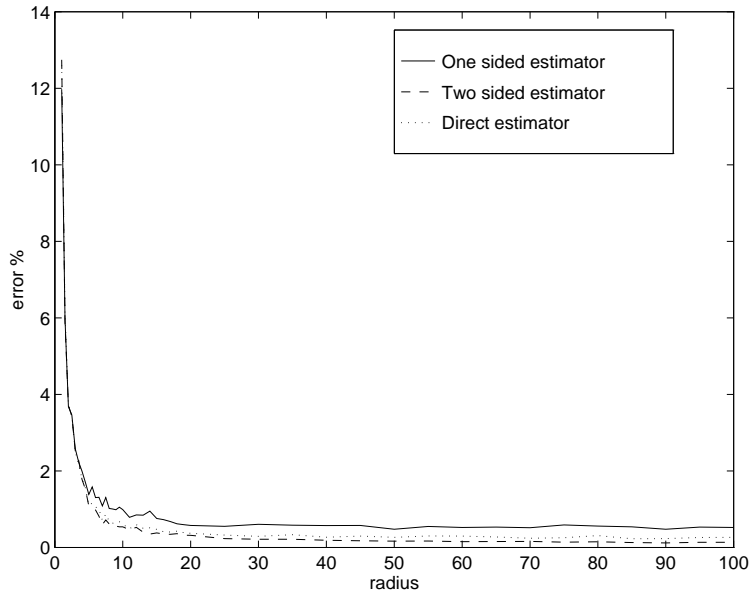


Figure 14: The RMS errors in perimeter estimation of circles using the three suggested estimators.

## 9 Discussion

Estimators for the original length of 3-D curves that are given in digital form are developed in this paper. Estimation is possible subject to the fundamental assumption that the quantization of the curve is sufficiently fine to capture the essential shape of the curve. In particular, following the standard design methodology developed in 2-D (see, e.g., [14]) and extended to 3-D [11], it is assumed that locally, along the curve, except at a small number of corners, the curve is sufficiently smooth to be considered nearly straight within  $3 \times 3 \times 3$  digital neighborhoods<sup>1</sup>.

The design principle is to derive an estimator from local properties of the digital curve, that will be unbiased and minimize an error criterion for straight lines. Unbiasedness for straight lines implies that in a general curve local estimation errors can be expected to largely cancel out due to the variability in tangent orientations along the curve. In this research, as in [11], the MSE criterion was used. It is possible to design similar estimators using other error criteria, such as the min-max criterion that was used in [14] for the development of 2-D perimeter estimators.

It should be stressed that to be applicable to general curves, the estimator should rely on *local* properties of the digital curve. In practice, estimation is based on classification of

---

<sup>1</sup>Near-straightness in smaller neighborhoods is sufficient for the one-sided estimator.

Estimator	RMS Error	Data source	Input
$\hat{L}_1$	2.49%	CQ	6-Chain
$\hat{L}_2$	0.57%	CQ	6-Chain
$\hat{L}_3$	1.13%	CQ	Digital image
$\hat{L}_{KK}$	2.88%	TCQ	26-Chain
$\hat{L}_{Ver}$	2.33%	Shortest Path	26-Chain
$\hat{L}_{BS}$	2.8%	Shortest Path	26-Chain

Table 3: The suggested estimators in perspective of previously available methods. The upper part shows the one-sided, two-sided and direct estimators developed in this work. The lower part presents the length estimator of Kiryati and Kübler, the results of Verwer and Beckers and Smeulders. Shown are the RMS error for straight lines, the data source - either a curve quantization method or, in the case of distance transforms, a shortest path algorithm, and the input format. Unlike the other works, Beckers and Smeulders defined the error per string element rather than per unit length. (Note that Verwer also presented a more accurate method that is based on finer classification of the chain elements of the shortest digital path. Unlike curve length estimation, in unconstrained distance transformations the shortest paths are always straight and locality of classification is of little importance).

chain code elements or digital curve points according to the structure of the digital curve in their neighborhood. Increasing the size of the neighborhood can lead to finer classification and better estimation of the length of *straight lines*, but when applied to general curves will lead to violations of the assumption that the curve is nearly straight within the (larger) neighborhoods.

An important purpose of the experiments is to provide data and insight about the failure modes of the suggested estimators as the smoothness assumption ceases to be valid. The classification support region for the two-sided estimator is larger than that of the one-sided estimator. It is thus not surprising that while the two-sided estimator is more accurate than the one-sided estimator when applied to circles of a radius larger than about 5, it has no significant advantage for smaller circles.

Some caution should be practiced in comparing the suggested estimators to those reported in the literature, see Table 3. We find limited interest in estimators that rely on global characterizations of digital straight lines rather than on local properties, since they are inapplicable to curves. (For example, one estimator considered in [3] is the Euclidean distance between the first and last digital point). The development of other estimators has been based on the erroneous claims that the line-to-arc and projection properties hold for 3-D GIQ and OBQ (Object Boundary Quantization). The results of [18] and [2] relate to the design of local weights for distance transformations, a problem that in 3-D is similar, but not identical, to

the design of length estimators. In particular, the digital paths obtained by a shortest path algorithm are necessarily digital arcs and are thus much simpler than digital straight lines obtained by 3-D GIQ, that are not digital arcs. To our knowledge, the only valid, non-trivial, 3-D length estimator that has so far been available is that of reference [11], but the 3-D digital curve representation scheme used there (TCQ) has certain limitations, notably the lack of direction symmetry.

To avoid these pitfalls, we first identified cube quantization as a mathematically well defined and well behaved 3-D curve representation scheme [9], then went on to develop 3-D length estimators based on cube quantization. The main difficulties that we had to overcome were in local classification of digital points in 6-chains, which is not as obvious as in 26-chains used in previous works, and in the cumbersome details of the development that necessitated the use of mathematical software. The estimators that were obtained, as presented in section 4, are easy to interpret and apply, and significantly outperform previous techniques.

## Acknowledgments

This research was supported in part by the Fund for the Promotion of Research at the Technion and by the Ollendorff Center of the Department of Electrical Engineering.

## References

- [1] T.M. Amarunnishad and P.P. Das, "Estimation of Length for Digitized Straight Lines in Three Dimensions", *Pattern Recognition Letters*, Vol. 11, pp. 207-213, 1990.
- [2] A.L.D. Beckers and A.W.M. Smeulders, "Optimization of Length Measurements for Isotropic Distance Transformations in Three Dimensions", *CVGIP: Image Understanding*, Vol. 55, pp. 296-306, 1992.
- [3] S. Chattopadhyay and P.P. Das, "Estimation of the Original Length of a Straight Line Segment from its Digitization in Three Dimensions", *Pattern Recognition*, Vol. 25, pp. 787-798, 1992.
- [4] L. Dorst and A.W.M. Smeulders, "Length Estimators for Digitized Contours", *Computer Vision Graphics Image Processing*, Vol. 40, pp. 311-333, 1987.
- [5] H. Freeman, "Boundary Encoding and Processing", in B.S. Lipkin and A. Rosenfeld (eds.), *Picture Processing and Psychopictorics*, pp. 241-266, Academic Press, New York, 1970.

- [6] H. Freeman, "Computer Processing of Line-Drawing Images", *Comput. Surveys*, Vol. 6, pp. 57-97, 1974.
- [7] E. Hlawka, *The Theory of Uniform Distribution*, AB Academic Publishers, Berkhamsted Herts, 1984.
- [8] A. Jonas and N. Kiryati, "Length Estimation in 3-D Using Cube Quantization", *Proc. SPIE Vision Geometry III*, Vol. 2356, pp. 220-230, Boston, 1994.
- [9] A. Jonas and N. Kiryati, "Digital Representation Schemes for 3-D Curves", Technical Report No. 114, Center for Communication and Information Technologies, Department of Electrical Engineering, Technion - Israel Institute of Technology, Haifa, Israel, July 1995.
- [10] C.E. Kim, "Three-Dimensional Digital Line Segments", *IEEE Trans. Pattern Anal. Machine Intell.*, Vol. PAMI-5, pp. 231-234, 1983.
- [11] N. Kiryati and O. Kübler, "On Chain Code Probabilities and Length Estimators for Digitized Three Dimensional Curves", *Pattern Recognition*, Vol. 28, pp. 361-372, 1995.
- [12] R. Klette, "The m-Dimensional Grid Point Space", *Computer Vision Graphics Image Processing*, Vol. 30, pp. 1-12, 1985.
- [13] J. Koplowitz, "On the Performance of Chain Codes for Quantization of Line Drawings", *IEEE Trans. Pattern Anal. Machine Intell.*, Vol. PAMI-3, pp. 180-185, 1981.
- [14] J. Koplowitz and A.M. Bruckstein, "Design of Perimeter Estimators for Digitized Planar Shapes", *IEEE Trans. Pattern Anal. Machine Intell.*, Vol. PAMI-11, pp. 611-622, 1989.
- [15] N. Kiryati and G. Székely, "Estimating Shortest Paths and Minimal Distances on Digitized Three Dimensional Surfaces", *Pattern Recognition*, Vol. 26, pp. 1623-1637, 1993.
- [16] A. Rosenfeld, "Three-Dimensional Digital Topology", *Inform. and Control*, Vol. 50, pp. 119-127, 1981.
- [17] I. Stojmenović and R. Tošić, "Digitization Schemes and the Recognition of Digital Straight Lines, Hyperplanes, and Flats in Arbitrary Dimensions", *Contemporary Mathematics*, Vol. 119, pp. 197-212, 1991.
- [18] B.J.H. Verwer, "Local Distances for Distance Transformations in Two and Three Dimensions", *Pattern Recognition Letters*, Vol. 12, pp. 671-682, 1991.